Thermal desalination from rejected heat of power cycles working with CO$_2$-based working fluids in CSP application: A focus on the MED technology

Michele Doninelli [a,*], Ettore Morosini [b], Giancarlo Gentile [b], Lorenza Putelli [a], Gioele Di Marcoberardino [a], Marco Binotti [b], Giampaolo Manzolini [b]

[a] *Università Degli Studi di Brescia, Dipartimento di Ingegneria Meccanica ed Industriale, Via Branze 38, 25123 Brescia, Italy*
[b] *Politecnico di Milano, Dipartimento di Energia, Via Lambruschini 4A, 20156 Milano, Italy*

ARTICLE INFO

ABSTRACT

This work analyses the integration of concentrated solar power plants based on innovative sCO$_2$ cycles and transcritical CO$_2$-based mixtures cycles with thermal desalination plants adopting the conventional MED technology. In these cogeneration plants, all heat rejected from the cycle is exploited by the desalination system, avoiding any parasitic electric consumption of the fans of the air-cooled heat rejection unit. The MED layout proposed exploits both latent effects, from 3 to 8, and sensible effects, to match at best the temperature level at which the heat is available from the power cycles, delivered to the desalination plant through an intermediate loop of demineralized water.

The cogenerative solution is designed in all its components and proposed in this work as a 100 MW$_{el}$ solar tower CSP plant located in Sevilla, resulting in a yearly production of around 400 GWh$_{el}$/year and between 3.5 and 4.2 Mm^3 of freshwater produced, depending on the configuration analysed. Various power cycle layouts are investigated, working with both sCO$_2$ and the innovative CO$_2$ + C$_6$F$_6$ mixture as working fluids. Regarding the solar plant, detailed models for the solar field optical analysis and the receiver thermal analysis are adopted. The seawater desalination plant, when coupled with this category of CSP plants, presents a thermal consumption between 180 and 140 kWh/m^3. Finally, the cogenerative plants performances are compared in terms of levelized cost of electricity, with a slight edge for the innovative mixture cycles, and levelized cost of water, in a range between 1 and 2 \$/m^3.

Introduction

The global water demand for all uses in the 2010s was about 4600 km^3 per year, with an estimated growth by 20–30% in 2050, up to 5500–6000 km^3 per year [1]. Today, 3.6 billion people live in areas with shortage of potable water at least one month per year, and this number is expected to increase to 4.8–5.7 billion by 2050 [2]. Desalination of seawater is a well-established technology adopted to reduce the mismatch between local clean water demand and the limited access to conventional water resources, but also to improve the quality of existing brackish water. In 2020 there were 16,876 installed desalination plants around the world (20971 including the ones under construction), representing an installed capacity of 97.2 million m^3/day [3]. Whilst desalination has great potential, there are barriers that limit its diffusion, such as capital costs, the related greenhouse gases emissions and the management of the produced brine.

Nowadays, the market share of thermal desalination technologies is about 33% of the total, while the membrane-based reverse osmosis (RO) dominates almost the rest of the market [4]. However, thermal desalination is the most applied technology in the Arabian Gulf countries covering about 68% of the installed facilities, due to its reliability in handling critical seawater conditions of high temperature and salinity [5]. The adoption of a thermal based technology avoids the necessity to periodically replace membranes, massively pre-treat the seawater and to shut down the plant for months in case of red tide phenomena [6]. The dominant thermal desalination technologies are multi-stage flash (MSF) and multi-effect distillation (MED), with MED normally preferred for the lower thermal and auxiliary electric energy consumption. The thermal energy consumption of a typical MED process powered by latent heat is

64 kWh/m^3 at a first effect temperature of 67 °C, whereas the MSF would require at least 105 °C to have the same specific energy consumption [7]. Nevertheless, the main issue related to MED processes are scaling phenomena that limit the top brine temperature under 70 °C, effectively narrowing the admissible operational temperature range.

Various MED plants are studied in literature adopting conventional steam Rankine cycles to deliver latent heat to the desalination system, usually through bleedings from the turbine, effectively leading to a parasitic load that reduces the electric efficiency of the power block itself. Under this perspective, a feasible application of Rankine cycles within the renewable energy spectrum is concentrated solar power (CSP).

As a matter of fact, among the many renewable energy technologies, CSP with thermal energy storage (TES) can be identified as one of the most interesting technologies to provide dispatchable and flexible electricity to the grid [8]. In particular, CSP plants based on the tower concept (i.e., solar tower) are particularly promising due to the high maximum temperature that can be reached by the heat transfer fluid (HTF). At the current state-of-the-art of solar tower plants, steam Rankine cycles are adopted to convert the thermal energy into electricity. Alternatively, supercritical CO_2 cycles (sCO_2) have been widely studied in literature to enhance the CSP competitiveness thanks to their smaller weight and volume and to simpler power block layouts [9]. However, a suitable power cycle for CSP applications should operate with high efficiency at high minimum temperatures of the cycle, especially if an air-cooled heat rejection unit is adopted: this key characteristic cannot be necessarily guaranteed with sCO_2 cycles due to their drop in cycle efficiency when the compression step is far from the critical point of the working fluid (around 31 °C). A possible solution, investigated in the H2020 SCARABEUS project [10], can be the adoption of CO_2-based mixtures as working fluids to turn the supercritical cycle into a transcritical one. Mixing carbon dioxide with a dopant that has a higher critical temperature compared with pure CO_2 (31 °C) allows having transcritical cycles also at high values of minimum temperature (above 50 °C), ensuring benefits in terms of efficiency and simplicity of the power block layouts [11]. Among the many possible mixtures for this purpose, $CO_2 + C_6F_6$ has been already considered for power cycles, in particular for CSP applications within the SCARABEUS project [12]. Moreover, the mixture has been safely proved to be thermally stable above 550 °C from an experimental perspective [13], a temperature level coherent with the current state of the art solar tower CSP plant with solar salts as HTF.

This work aims at evaluating the potentiality of a CSP + MED cogeneration system for the simultaneous production of electric energy and demineralized water, where a CO_2-binary mixture is adopted as working fluid in the power cycle. After the modelling of all the components at design conditions, an annual analysis is carried out to compare the performance of difference cycle layouts and the results of a pure sCO_2-based cycle. Differently from this work, literature works typically provide techno-economic analyses of CSP + D systems not based on yearly analysis, but only considering the design conditions. Performance maps of the specific thermal energy consumption of a MED plant powered by a low-temperature sensible heat source are also provided, which could be useful to assess the potentiality of a coupling between a different sensible waste heat source (such as heat recovery before the stack of a combined cycle in the range above 45 °C). As a matter of fact, in this work the low-grade heat is introduced in the MED system with an intermediate water loop of demineralized water above 45 °C, which is the minimum value compatible with the MED technology, since the last MED effect is typically at a temperature around 40–44 °C. Economic results are also provided, with maps of the levelized cost of water (LCOW) as function of MED layout, the temperature of the sensible heat source and plant capacity factor, which could be useful for the performance assessment in other locations.

Compared to other literature works, in this analysis the rejected heat from the cycle is fully exploited in the desalination unit, thus avoiding both the electrical consumption of an additional air-cooled condenser and avoiding any electrical production losses, that would be unavoidable with steam Rankine cycles due to the bleeding from the low-pressure steam turbine that feed the MED plant.

The complete and detailed modelling of the entire CSP + D system, including the MED system, the solar field, the thermal receiver, the consumption of the HTF pump and the power cycle is a key factor to accurately estimate the LCOW based on real total equivalent annual operating hours. Ultimately, this work will present the performances of a CSP + MED plant in terms of levelized cost of energy (LCOE) and LCOW considering Sevilla (Spain) as a suitable location, since it is representative of a of a European location with high irradiance, for a power plant with an electric output of 100 MW_{el}.

Literature review on the coupling between CSP and MED systems

The coupling between a low-grade renewable heat source and MED systems has been studied in the literature, not only through the
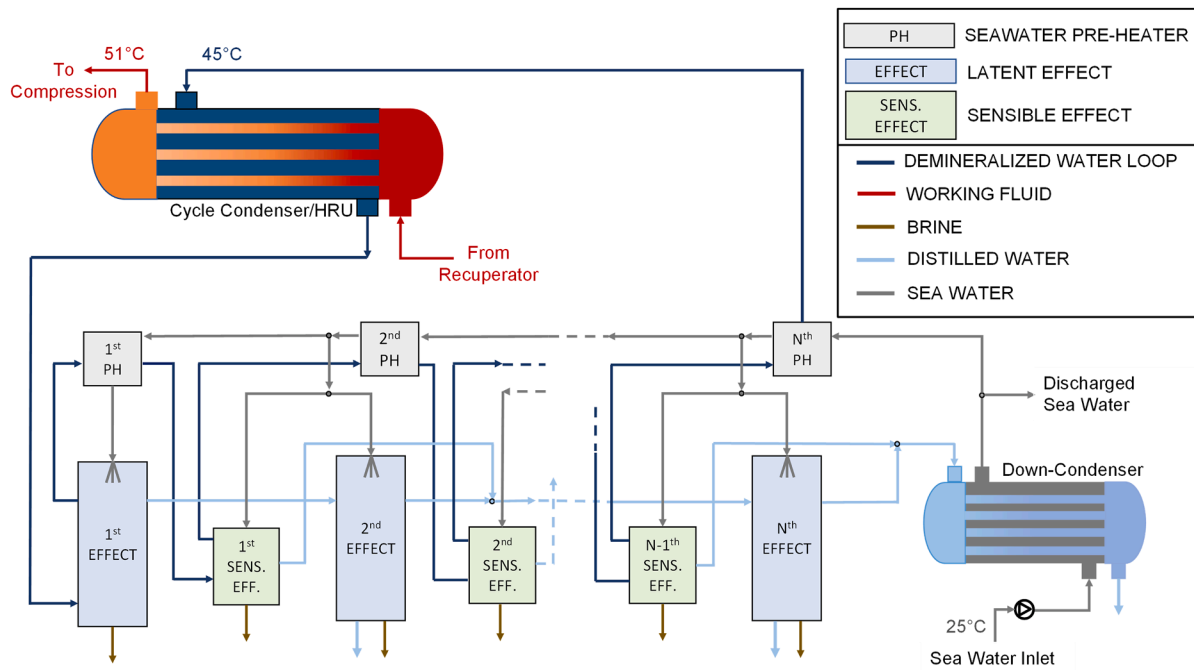
Fig. 1. Plant layout of the MED plant adopted in this work.

integration with power cycles but also with salt gradient solar ponds [14] or with solar collectors and thermal energy storage systems [15] proving to be an effective solution in semi-arid regions. In their review, Ahmed et al. [16] emphasized the need for comprehensive studies on hybrid CSP power systems and desalination plants, also underlining the importance of using available waste heat to improve the economic performance of the plants. An integrated and cogenerative CSP and desalination system (CSP + D) has been proposed and described by Moser et al. [17] from a financial and environmental point of view. Palenzuela [18] carried out a techno-economic comparison between CSP + MED and CSP + RO systems in Mediterranean and MENA regions, and the integration between MED and CSP resulted to be the most favourable in dry cooling conditions. Sankar [19] studied the carbon black industry where both electricity and freshwater are required, concluding that the coupling between CSP and MED yields higher economic benefits and ensures production continuity compared to the round the clock production of the CSP + RO system. In another work, Olwig [20] compared two hybrid CSP + TVC + MED and CSP + RO systems operating with 42 MW steam Rankine cycles powered by a parabolic through CSP plant, resulting in better economic performance for the CSP + RO configuration, with LCOW of about 1\$/m^3 computed with feed-in-tariff of 240\$/MWh$_{el}$ for the electricity share. It is nevertheless necessary to underline that the LCOW, in case of the CSP + RO hybrid system, is strongly dependent on the electricity price. Askari [21] studied a linear Fresnel powered steam Rankine cycle integrated with either MED, RO, TVC + MED and the separate freshwater production by coupling directly MED and TVC + MED with the solar field: the LCOW computed was around \$1.6/m^3 for the CSP + MED cogeneration plant and \$3.1/m^3 for the separate production. Finally, the attractivity of this cogenerative solution has been demonstrated not only in CSP hybrid plants: for example Moradi et al. [22] studied a hybrid system for combined electric power and freshwater production where the heat from a solid oxide fuel cell is recovered by a Stirling engine providing steam for a multi-effect desalination unit.

As mentioned, in traditional power plants coupled with MED plants, steam is expanded in backpressure turbines with associated power loss of about 3 kWh$_{el}$/m^3 of freshwater [23]. Sharaf et al. [24] analysed a hybrid system composed by a solar ORC and a MED-VC (vapour compression), where the thermal or mechanical compression of the

vapour feeding the first effect of the MED improves its thermal energy consumption and increases the water production rate. However, both the systems have drawbacks: the ejector of the thermal vapour compressor requires feeding motive steam that must be generated in a separate boiler by scarifying thermal energy collected from the solar field, while the mechanical vapour compression requires the use of electrical power generated by the solar ORC to power a compressor. The option of increasing the minimum cycle temperature of the ORC to directly reject the latent heat of condensation to the MED unit is totally counterproductive from the efficiency point of view.

Moving from steam cycles to innovative cycles, both for sCO$_2$ and CO$_2$-based mixtures power cycles in CSP applications the heat is rejected at a relatively high temperature (above 80 °C, depending on the mixture and the assumptions on the cycle characteristics). This large contribution of thermal power, released to the environment with air cooled heat rejection unit (HRU), can be instead used under a cogenerative perspective in a thermal desalination plant for potable water production: in fact, the non-isothermal heat rejection fits the needs of the thermal level required by the desalination plant, without the need to compromise the net electrical power output. The coupling between the cycle HRU and the MED unit can be achieved with a closed loop of demineralized water that absorbs the heat from the cycle and releases it to the MED system. The coupling between CSP and MED has a twofold beneficial effect: the exploitation of the cycle wasted heat to produce fresh water and the adoption of a water-cooled HRU instead of an air cooled one, with a consequent reduction of the capital and operating cost (avoiding the consumption of auxiliary fans for dry cooling).

In recent years, the study of sCO$_2$ cycles coupled with MED plants has been carried out by a series of authors in the literature [7,25,26]: in those cases, the cycle minimum temperature considered was around the critical temperature of CO$_2$, to exploit real gas effects and optimize the cycle efficiency. Under this assumption: i) not all the available wasted heat from the cycle could be exploited by the desalination plant, since the temperature of the heat introduction to the MED system is limited above 40 °C by the seawater temperature preheated in the down-condenser, ii) the design and operation of the compressor of the sCO$_2$ cycle becomes critical [27]. In contrast, a higher value of minimum cycle temperature (51 °C) is assumed in this work: this temperature is suitable to describe high ambient temperature locations, enabling to maximize

Table 1
Assumptions on the seawater conditions and the MED plant.

Parameter	Value
Seawater salinity [g_{SALT}/kg_{WATER}]	35
Seawater temperature [°C]	25
Rejected brine salinity [g_{SALT}/kg_{BRINE}]	70
Last effect temperature [°C]	44
Demineralized water inlet temperature [°C]	45
Pinch point between sensible effects [°C]	3
ΔT between latent effects [°C]	3–4

the cogeneration production of the CSP + D plant, and at the same time to explore the potentiality of CO_2-mixtures as working fluid in transcritical cycles for electrical and potable water production.

Methodology: MED system

As discussed, MED plants are a flexible and reliable solution for seawater desalination in case low-grade heat is available. The layout of the process is ideally composed of a cascade of effects (or stages) where a sequence of simultaneous evaporation and condensation processes occurs, obtained by spraying preheated seawater on the top of a tube bundle in which the condensation of the vapour formed in the previous effect takes place.

The specific MED layout and the coupling between the power cycle HRU and the MED are depicted in Fig. 1, assumed according to literature [26] for this application and composed of a series of latent and sensible effects. As already mentioned, the heat transferred to the desalination plant is the totality of the rejected heat from the power cycle enabling an efficient coupling between the two systems. The thermal power is exchanged through an intermediate closed loop of demineralized water that represents the cold sink for the cycle and at the same time the hot source for the MED. The demineralized water enters the heat rejection unit (HRU) at 45 °C and exits at a temperature that depends on the power cycle characteristics, but always higher than 70 °C. The intake seawater enters the down-condenser, acting as a coolant, to allow the condensation of the distilled water vapour produced in the last (Nth) effect assumed at 44 °C (last effect temperature, bottom brine temperature). The necessary seawater to completely condense, in the down-condenser, the water evaporated in the last latent effect is higher than the seawater that can be treated in the MED: hence, a part of it is discharged after the down-condenser. The other stream of seawater feeds the MED unit. In particular, it is preheated to saturated conditions by the demineralized water in the last (Nth) preheater. After that, a fraction of preheated seawater enters both the last effect (Nth) and the last sensible effect (N-1th) to evaporate. In particular, the preheated seawater is evaporated in the sensible intermediate effect due to the heat released by the sensible demineralized water loop (with pinch point temperature difference as reported in Table 1), while in the main effect evaporation occurs through the latent heat of condensation of the vapour formed in the previous effect. The desalinated water vapour produced in both the

last sensible and main latent effects are then condensed in the down-condenser. The other fraction of preheated seawater, that is not sent to the last stage, is further preheated to reach saturation conditions at a temperature higher than the one in the previous preheater. As before, a fraction of seawater is evaporated in the sensible and latent effects, while a part is sent to the next preheater. The difference between the last effect and the previous ones is that the steam produced in the previous effects is not condensed with seawater in the down-condenser but is condensed into the subsequent latent effects. In fact, in the latent effects occur simultaneously the condensation of this steam and the evaporation of preheated seawater.

The operating principle is repeated in each effect except for the first effect, where evaporation of seawater (at the maximum temperature, the top brine temperature, limited under 70 °C due to scaling issues) occurs exclusively by means of heat transfer from the demineralized water loop.

The temperature of the vapour formed in the first effect depends on the number of effects considered. In this study, MED units from 3 to 8 effects are considered, with a temperature difference of 3 °C and 4 °C between each latent effect.

The thermodynamic performances and the economic analysis of various configurations of MED plants, under different conditions and number of effects, have been evaluated under the assumptions of Table 1. The salinity of the rejected brine and the other operating parameters and constraints are controlled by including upper bounds. To avoid scaling issues, the salinity of the rejected brine is limited by the vapor quality imposed at 50% at the outlet of each latent effect: the evaporated half fraction (salt-free) is condensed in the subsequent latent effect, while the other half liquid stream (with a salinity of two times the seawater) is directly rejected, called brine. The split ratio after each preheater (controlling the seawater entering the latent effect, sensible effect and subsequent preheater) is calculated iteratively to simultaneously meet the constraints on the pinch temperature difference in the sensible effect and on the vapour fraction in the latent effect.

Sharan et al. [26] demonstrated that the adoption of intermediate sensible evaporators in a MED unit powered by a sensible heat source is beneficial to increase the distillate production. This solution has been applied in this work because it allows to cool the demineralized water loop down to 45 °C, as required considering the characteristics of the power cycles.

The MED system and its coupling with the sensible heat source (demineralized water) are simulated in Aspen Plus V12 [28] as already done in the literature [29]. The thermodynamic properties of the seawater, treated as a mixture of water and sodium chloride (NaCl), are modelled with the electrolyte Non-Random Two-Liquid (NRTL) model with Redlich-Kwong equation of state.

Additional details on the plant proposed in Fig. 1 for a case specific condition, representative of a real plant, are proposed Appendix A, along with some considerations on the technology adopted for the effects and heat exchangers of the MED plant.
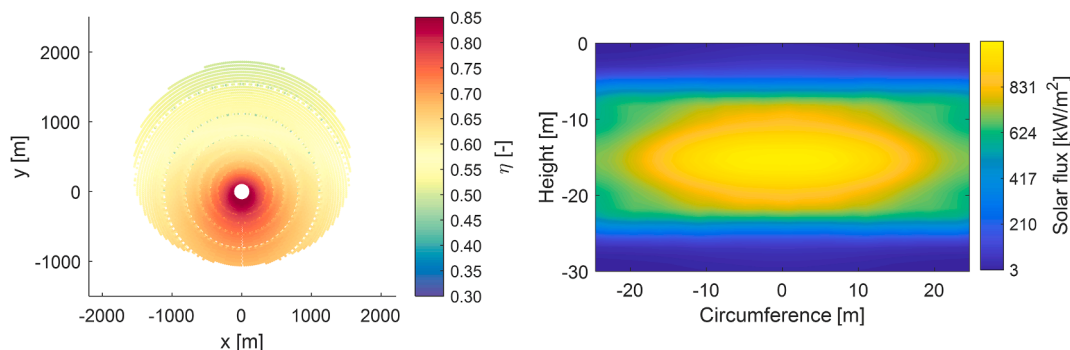
Fig. 2. Planar view of the solar field from SolarPilot: heliostats optical efficiency characterization (left). Thermal flux on the receiver at design conditions (right).

Table 2

Receiver dimensions and tube circuitations of the two configurations of tubular receiver considered in this work, adopting solar salts as HTF.

	Low HTF inlet temperature	High HTF inlet temperature
HTF inlet/outlet temperature [°C]	290 / 565	420 / 565
HTF	Solar Salts	
Receiver height [m]	30.5	
Receiver diameter [m]	15.8	
Design thermal input ($\dot{Q}_{in,rec}$) [MW$_{th}$]	717	
Coating absorptivity [%], emissivity [%]	93, 87	
Tubes material	Haynes 230	
Tubes spacing [mm]	2	
Tube outer diameter / thickness [mm]	51.5 / 1.65	75.5 / 2.1
Tubes per panel / panels per flow path [-]	66 / 7	40 / 8
Performances on design conditions		
HTF mass flow rate [kg/s]	717	1350
Pressure drop on the receiver [bar]	16.7	30
HTF pump consumption [MW$_{el}$]	2.54	6.05
Receiver thermal efficiency [%]	85.44	85.37

Methodology: CSP plant modelling

The MED system is assumed to be coupled with a 100 MW$_{el}$ CSP plant based on a solar tower receiver and located in Sevilla, Spain. The solar field, which is fixed for all the power cycles considered in this work, is generated through SolarPilot [30] assuming a design thermal input to the receiver of 717 MW$_{th}$ and considering the same tower height, heliostats dimensions, receiver height and receiver diameter of the Crescent Dunes power plant, located in Tonopah (NV, USA) [31]. Appendix B reports some of the details on the methodology adopted for the design and simulation of the CSP Plant. The solar field aerial view and the optical efficiency of each heliostat is depicted in Fig. 2 (left), while the obtained heat flux map on the receiver at design conditions (summer solstice, solar noon, DNI of 950 W/m^2) is shown in Fig. 2 (right).

Regarding the receiver design, two different conditions are considered at constant receiver height and diameter and assuming two separate flow paths of the HTF (one on the east side, the other on the west side). The first design, considered for the scenario with HTF temperature at the receiver inlet equal to 290 °C, has the same characteristics of the Crescent Dunes receiver; the second design, that is adopted for the cases with HTF temperature at the receiver inlet in the range 415 °C–432 °C, much higher than in the Crescent Dunes plant, has the same receiver

height and diameter of the first one, but with different tubes dimensions and arrangement. Once the geometry of the receiver and the solar field are determined, the receiver thermal efficiency is computed with the Modelica package SolarReceiver2D [32]. Additional details on this thermal analysis and the modelling of the receiver circuitation for the second receiver are available in Appendix B. The performance of the receiver in both conditions are reported in Table 2, along with the main assumptions on the receiver geometry, the tube materials, spacing, absorptivity and emissivity.

To carry out the yearly analysis, the thermal efficiency in off-design conditions is only determined by the thermal power on the receiver, as suggested in literature [9]. The calculations in off-design are carried out with the same thermal model adopted for the design calculations, scaling the input heat flux map. Fig. 3 reports the trends of receiver thermal efficiency and HTF pump electric consumption as function of the ratio between receiver thermal input ($\dot{Q}_{in\,rec}$) and design thermal input ($\dot{Q}_{in\,rec,design}$).

Methodology: Power cycles simulations

In recent years, sCO$_2$ cycles have been studied for application in CSP plants in various configurations, evidencing the recompression layout as optimal for the coupling with CSP, mainly due to the high cycle efficiency [33]. Nevertheless, considering the state-of-the-art HTF (solar salts) with maximum temperature of 565 °C, sCO$_2$ cycles are not particularly competitive with respect to steam cycles, mainly due to the limited temperature difference across the primary heat exchanger, leading to HTF temperature differences in the order of 150 °C [34]. The adoption of CO$_2$-based mixtures in transcritical cycles helps shifting this paradigm: due to a lower compression outlet temperature and more balanced heat capacities in the recuperator, they present a more limited drop in cycle efficiency at lower heat introduction temperatures than sCO$_2$ cycles. For this reason, in this work the CO$_2$ + C$_6$F$_6$ mixture is adopted both in plant layouts with high cycle efficiency and in the cascade layout, a specific configuration adopted to increase the heat recovery capability of the simple recuperative cycle.

The various cycle layouts considered are represented in Fig. 4. The cascade (CAS), the simple recuperative (SIM) and the precompression (PRE) cycles are analysed for the CO$_2$-mixture, already shown very promising for the selected working fluid in literature, particularly in CSP applications [35]. In addition, as reference case, the recompressed (REC) cycle is also investigated with sCO$_2$, since it is the most studied layout for CSP applications. Details on the power block layouts and simulations are discussed in Appendix C, while the necessary assumptions on the cycle non-idealities are shown in Table 3. In the simulations, the gross mechanical power is always set at 100 MW, the turbine inlet temperature is set to a typical value for the CSP plants using solar salts, while the minimum cycle temperature is assumed to be higher than 50 °C,
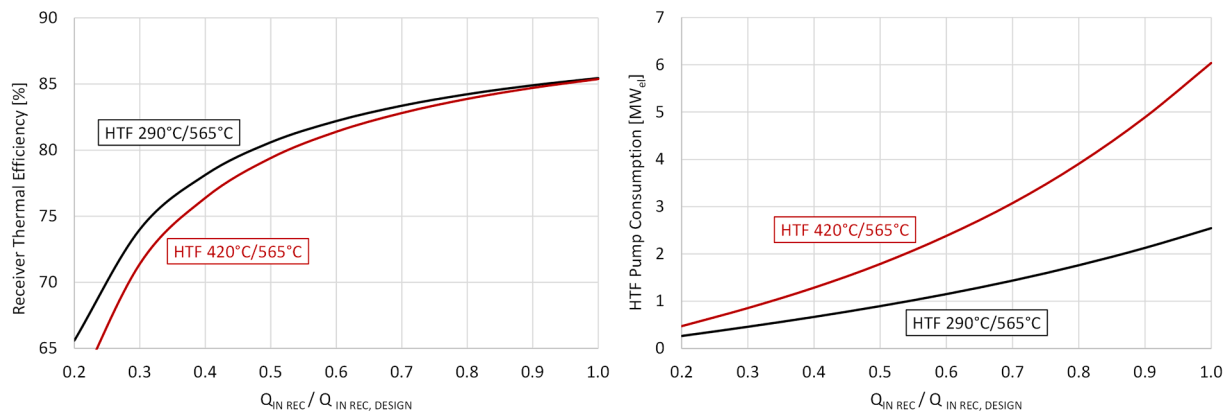
Fig. 3. Receiver thermal efficiency for the two circuitations presented in Table 2 (left). HTF electric pump consumption for the same conditions (right).
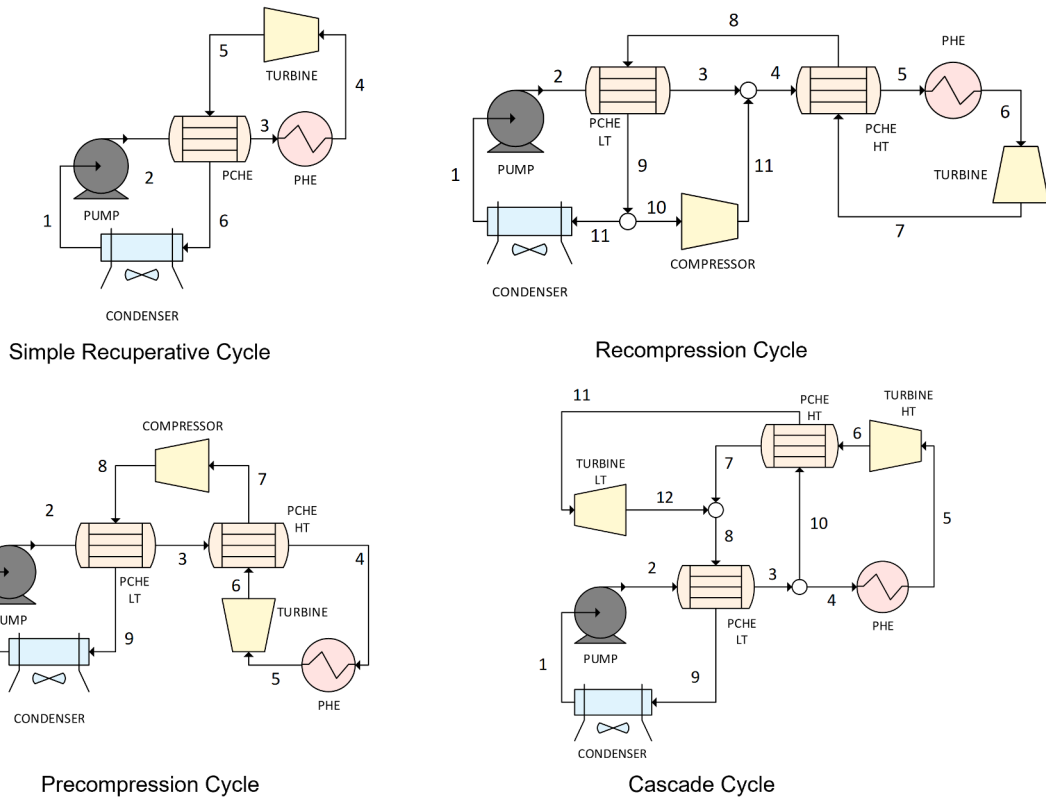
Fig. 4. Power block layouts considered in this work for the CO_2-based cycles.

Table 3
Power cycles assumptions and non-idealities.

Power Cycle Parameter	Value
Turbine Inlet Temperature [°C]	550
Turbine Inlet Pressure [bar]	250
Compression Inlet Temperature [°C]	51
Turbine / Compression Isentropic Efficiency [%]	92 / 88
PCHE Minimum Internal Temperature Difference [°C]	5
Condenser/ HRU Pressure loss [bar]	2
PHE Pressure loss [bar]	4
PCHE Pressure loss HP / LP [bar]	0.5 / 1

consistently with dry cooling in hot environments and to enable an efficient coupling with the MED plant, as shown in Fig. 1. The assumptions on the turbomachinery and heat exchangers are aligned with previous works and with the state-of-the-art technologies [36]. The Span-Wagner equation of state [37] is used for the thermodynamic properties assessment of the sCO_2, while the PC-SAFT equation of state with optimized interaction parameters is considered from literature [38], used to describe the thermodynamics of the $CO_2 + C_6F_6$ mixture.

As previous works evidenced [36], the advantage in term of economic performances of transcritical simple-recuperated CO_2-mixture cycles with respect to the recompressed sCO_2 cycles are evident especially at high minimum temperature, where pure CO_2 is far from the critical point and the compressibility factor sharply increases. The mixture composition, reported in Table 5, is selected optimizing the thermodynamic efficiency for each plant layout adopting the $CO_2 + C_6F_6$
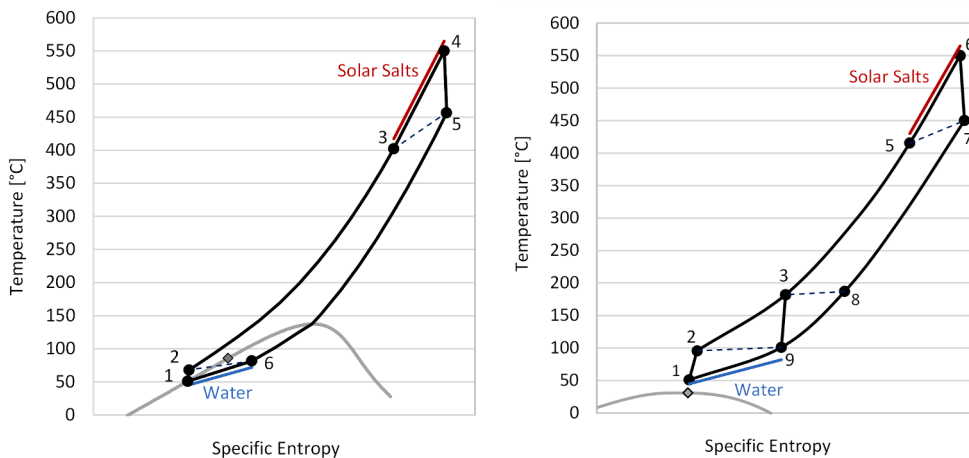

Fig. 5. T-s diagrams of the two power cycles proposed in Table 4: simple cycle with $CO_2 + C_6F_6$ mixture (left), sCO_2 recompressed cycle (right).

Table 4

Performance of two representative power cycles investigated in this work, including the thermal and mechanical power balance.

Variable	sCO$_2$ Cycle	CO$_2$ + C$_6$F$_6$ Cycle
Plant layout	Recompressed	Simple Recuperative
Mass Flow Rate [kg/s]	1410	1218
Specific Work [kJ/kg]	71.5	82.1
Pump/Main Compressor Power [MW]	31.0	25.0
Recompressor Power [MW]	22.6	–
Turbine Power [MW]	153.6	125.0
Recuperator Thermal Power [MW]	163 (LT) − 436 (HT)	623
PHE Thermal Power [MW]	237.8	238
HRU Thermal Power [MW]	137.8	138
UA$_{PCHE}$/PHE Thermal Power ratio [1/K]	0.22	0.15
Working fluid inlet PHE Temperature [°C]	416.6	401.1
Working fluid inlet HRU Temperature [°C]	100.4	81.7
Gross Cycle Efficiency [%]	42.8	42
Electromechanical losses [MW$_{el}$]	2	1.5
Cycle Electric Efficiency [%]	42.0	41.4

Table 5

Cycles investigated in this work: focus on the heat introduction (by the HTF) and heat rejection (in the HRU) processes.

	Dopant molar fraction [%]	Cycle gross efficiency [%]	HTF temperatures [°C]	Working fluid at HRU inlet [°C]	Temperature range demineralized water [°C]
SIM cycle	13% C$_6$F$_6$	42.0	420–565	81.9	45–72.0
PRE cycle	12% C$_6$F$_6$	43.3	415–565	81.4	45–71.3
CAS cycle	12% C$_6$F$_6$	39.5	288–565	82.7	45–72.7
REC cycle	Pure CO$_2$	42.8	432–565	100.4	45–82.2

mixture. The minimum pressure of the transcritical cycles working with the CO$_2$ mixture is the bubble pressure at pump inlet conditions, while it is an optimised parameter in case of sCO$_2$.

As the possibility to employ an efficient simple recuperated layout represents one of the most attractive features of CO$_2$ mixtures compared to sCO$_2$, Fig. 5 and Table 4 represent an insight on the comparison between the simple recuperative CO$_2$ + C$_6$F$_6$ cycle and the recompressed sCO$_2$ cycle, for a gross mechanical power of 100 MW.

In Table 5 are listed the key performance indicators of the various power block investigated in this work, along with the maximum temperature reached by the demineralized water in the hot side of the condenser, assuming a pinch point of 3 °C between the working fluid and the cooling flow of demineralized water. The heat rejection process from the power cycle to the closed loop (in the top left of Fig. 1) under these constraints is shown in the T-Q diagrams of Fig. 6, again for the simple recuperative cycle with the CO$_2$ + C$_6$F$_6$ mixture and the recompressed sCO$_2$ cycle: from the figure it is clearly visible that higher maximum temperatures of the demineralized water intermediate flow are possible with sCO$_2$ cycles, allowing for a more performant coupling between the power cycle and the bottom desalination plant.

Methodology: Yearly analysis

Once the methodology to model the CSP + D plant is presented, the yearly analysis is also detailed and described in this chapter, as the focus of this work is to determine the yearly performances of the cogenerative plants.

Since the cycles and the MED plant are decoupled by the demineralized water loop, the inlet and outlet conditions of the working fluid across the HRU are assumed to be always constant, in order not to influence the specific freshwater production. To do so, the power cycles must run always at constant load (full load), when thermal input is available in the HTF from the solar field, and always at constant cycle minimum temperature. In fact, a partial load condition would: i) penalize the cycle efficiency with respect to a full load condition, reducing the electric power produced, ii) decrease the inlet temperature of the working fluid in the HRU, meaning that not all the heat rejected would be available at a temperature range above 45 °C in the demineralized water loop. Since running the cycle in part load and decreasing the cycle minimum temperature would negatively affect the specific thermal consumption of the MED system, these two conditions are not considered.
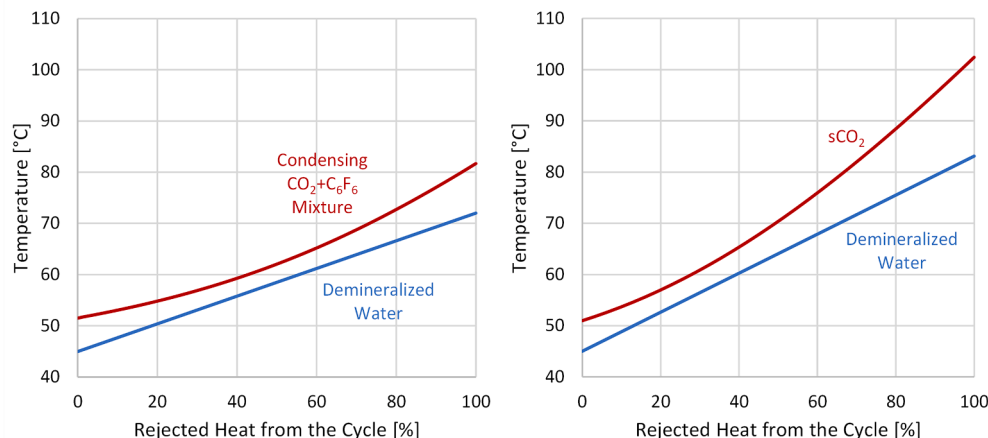
Fig. 6. T-Q diagrams of the HRU of the two power cycles presented in Table 4.
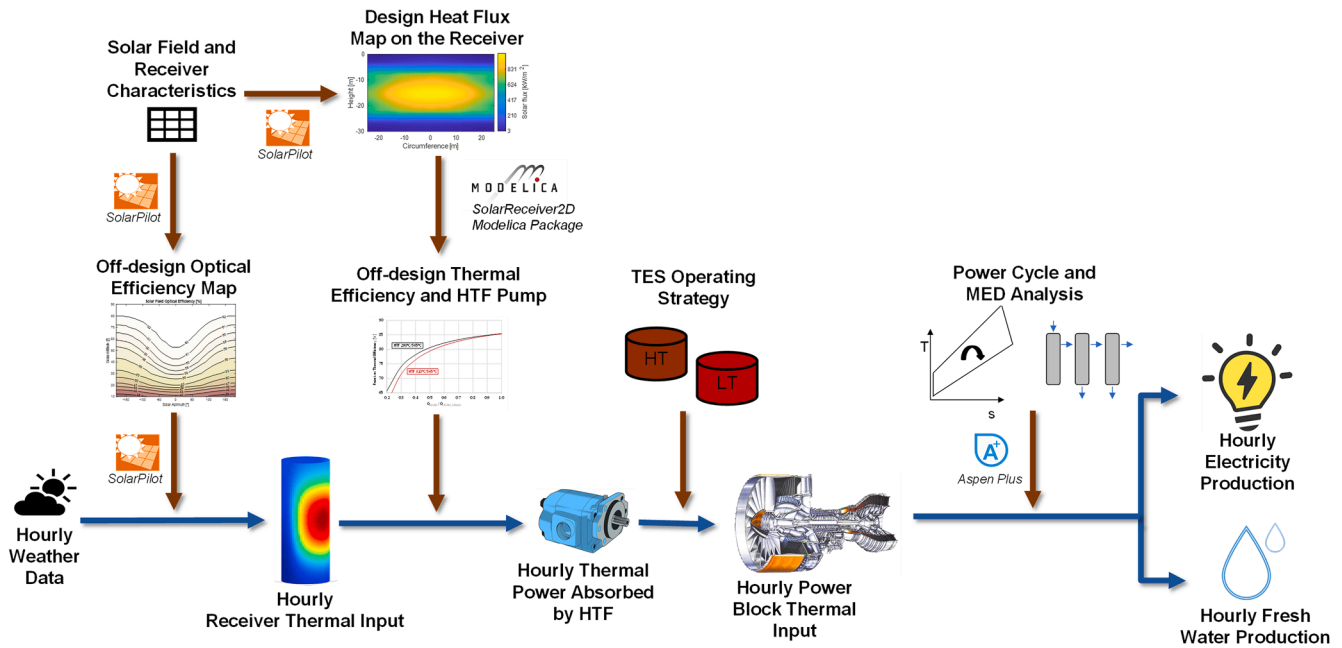
Fig. 7. Flowchart of the yearly analysis proposed in this work on an hourly basis.

An overview of the yearly analysis carried out in this work is represented in Fig. 7: starting from the hourly DNI data (available in the SolarPilot database for Sevilla and detailed in Appendix D), the optical efficiency of the solar field is evaluated for each sun position (reported in Appendix D). Then, according to the thermal model already presented and the results of the receiver thermal efficiency in Fig. 3, the thermal power absorbed by the HTF is computed for each hour of the year. Adopting a simplified TES operating strategy, the thermal power fed to the power cycle is computed: in case the power block is running at full load and the hot tank of the TES is full, a partial defocusing of some heliostats is assumed, to reduce the receiver thermal input. The TES size, on the other hand, is computed for each power cycle based on the optimal LCOE condition.

Ultimately, it is carried out an hourly analysis of the electric energy and the thermal energy rejected to the MED system. Coupling each power cycle with the intermediate loop of demineralized water, as presented in Table 5, allows to define the specific thermal consumption of the MED, univocally determined for each demineralized water maximum temperature and number of MED effects, as evidenced in the next section. Accordingly, the yearly overall energy produced and the yearly overall freshwater produced are determined for each power cycle investigated, with the solar plant proposed in this work.

Economic analysis

To correctly estimate the techno-economic performances of the cogenerative CSP + D plants, capital cost functions must be selected from literature. The euro-to-dollar conversion is applied, if necessary, with the average conversion factor of 2021. Costs functions are actualised to 2021 considering the Chemical Engineering Plant Cost Index (CEPCI) index. About the MED plant, the LCOW has been evaluated considering both the capital (CAPEX) and operating (OPEX) costs under the different operating conditions (heat source temperature, number of effects, heat input) according to Eq. (1).

$$LCOW\left[\frac{\$}{m^3}\right] = \frac{MED\ Plant\ CAPEX \cdot CRF\ +\ MED\ Fixed\ OPEX}{Yearly\ Fresh\ Water\ Produced} \quad (1)$$

Table 6
Economic assumptions for the cost model of the MED system.

Parameter	Value
Discount rate / CRF [40]	8% / 8.88%
MED Plant lifetime	30 years
Electric energy cost	150 $/MWh$_{el}$
Chemicals cost [41]	0.024 $/m$^3_{seawater}$
Labour cost [41]	0.05 $/m$^3_{seawater}$

The correlation developed by Kosmadakis et al. [39], fitted on over 28 existing MED plants, has been used to evaluate the CAPEX of the MED system as a function of the daily distillate product and the evaporator/condenser area. The estimation of the heat transfer area is relevant for the capital cost assessment, since the evaporator/condenser bundles consist of a large portion of plant's cost. A 20% increment factor has been applied to the calculated area of the latent effects to consider the realistic mean temperature difference due to thermodynamic losses that have been estimated under the geometry assumptions for the tube bundle in Appendix A.

The annual operating costs are evaluated considering the total equivalent operating hours of the CSP plant, including the characteristics of Table 6, such as: the cost of chemicals necessary to pre-treat the seawater, the direct labour cost and the electricity pumping cost of the seawater from the intake (assuming a total head developed of 3.5 bar), of the brine and distillate products, and of the demineralized water in the closed loop (assuming a pressure drop of 1 bar across the MED plant).

Regarding the CSP plant, the LCOE is computed accounting for the formulation of Equation (2):

$$LCOE\left[\frac{\$}{MWh_{el}}\right] = \frac{CSP\ Plant\ CAPEX \cdot CRF\ +\ CSP\ Fixed\ OPEX}{Yearly\ Net\ Electric\ Energy\ Produced} \\ + CSP\ Variable\ OPEX \quad (2)$$

To estimate the LCOE, specific cost functions are necessary for each of the plant components. For the power block, the cost of turbines, pumps, compressors, and recuperators are taken from Weiland [42],

while for both PHE and water-cooled condensers/HRU the cost functions from Weiland are not applicable. To estimate their costs, the two heat exchangers are modelled in Thermoflex [43] as shell and tube HX fitting the pressure drops of Table 3, adopting Inconel 617 for the tubes of the PHE and carbon steel for the tubes of the HRU, since the HX capital cost are provided by the tool.

The cost functions of the solar tower, receiver, HTF pump and HTF piping are taken from Kelly at al [44], actualized with the CEPCI index at the year 2021, and resulting in capital costs very similar to the ones proposed by System Advisor Model (SAM) [45]. The solar field cost, instead, is assumed equal to 140 $/m^2 of heliostat area as suggested in SAM. The TES cost, modelled as a direct two tanks solar salts system, is computed considering the cost analysis presented in Manzolini et al [46].

Additional financial assumptions and OPEX related to the CSP plant are listed in Table 7, mainly assumed from SAM.

Table 7
Financial assumptions for the cost model of the CSP plant.

| Parameter	Value
Discount rate / CRF	8% / 8.88%
CSP Plant lifetime	30 years
Fixed OPEX [$/kW/year]	66 $/kW/year
Variable OPEX [$/MWh$_{el}$]	3.5 $/MWh$_{el}$
CSP Indirect + Contingency Costs	20% of the overall CSP CAPEX

Results

In this chapter the thermodynamic and economic performances of the cogenerative CSP + D plants based on solar tower CSP plants are evidenced and discussed.

At first, the specific thermal consumption of the investigated MED system, proposed in Fig. 1, is shown in Fig. 8 as function of the number of latent effects and the maximum temperature of the demineralized water: the results assumed a 3 °C temperature difference between the latent effects as this condition is considered preferable (by around −15%) with respect to the one with 4 °C of temperature difference between latent effects.

Accordingly, the temperature of the demineralized water (heat source for the MED plant) considerably affects the thermal energy consumption and, thus, the instantaneous and annual production of freshwater. Fixing the number of effects, the thermal consumption decreases with the increase of the temperature of the heat source due to a larger percentage of heat introduced in in the first latent effect, whose steam product drives the evaporation of the seawater in the following stages.

On the other hand, the total equivalent annual operating hours (EOH) of the CSP power plant plays a significant role for the annual analysis. In a CSP plant, the annual EOH depends mainly on the weather data and the design choices of TES size and solar multiple. Since the LCOW, as expressed in Equation (1), is strictly related to the annual fresh water produced, its value depends on the location in which the solar
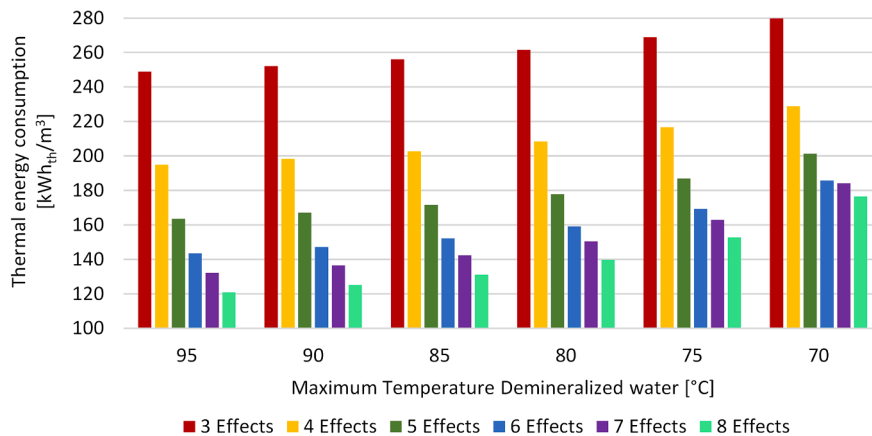
Fig. 8. Specific thermal energy consumption per unit of freshwater (m^3) produced with the MED plant described in this work (as in Fig. 1), with return temperature of demineralized water equal to 45°C (see Appendix A).
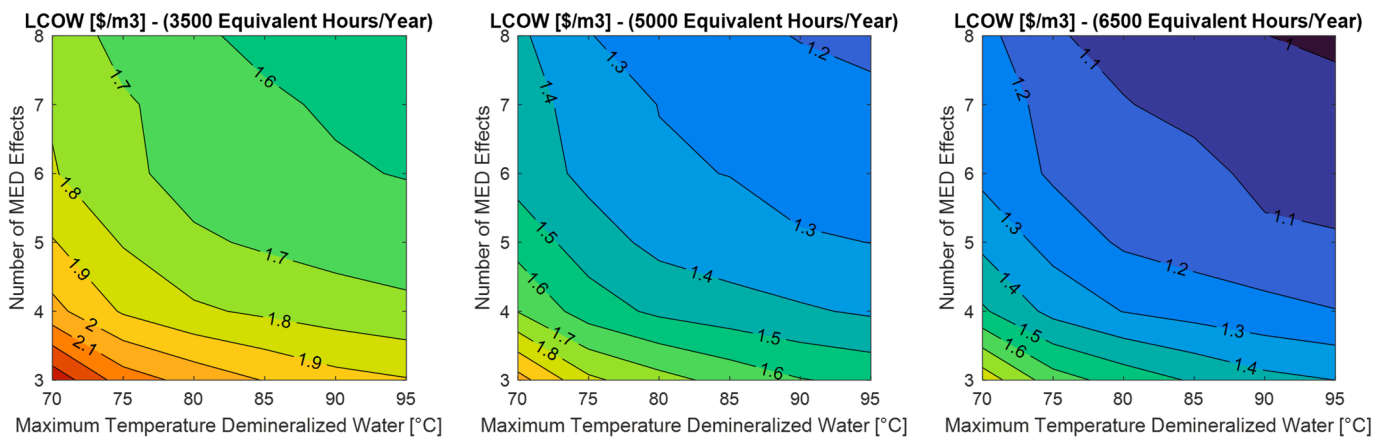
Fig. 9. LCOW [$/m^3] of freshwater produced with the MED plant in Fig. 1, as function of the number of MED effects and maximum temperature of demineralized water. Results for $\Delta T_{effects} = 3°C$.
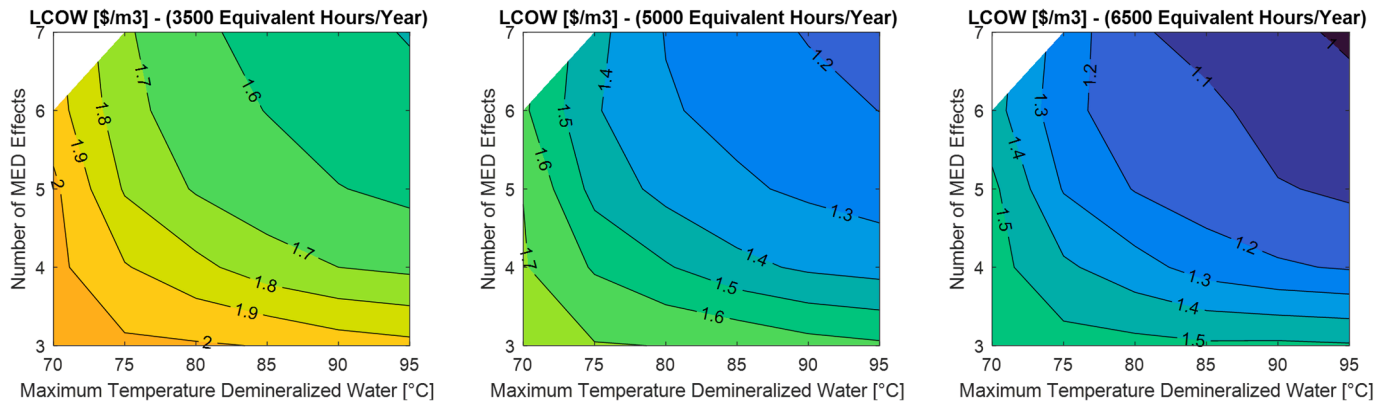
Fig. 10. LCOW [\$/m³] of freshwater produced with the MED plant in Fig. 1, as function of the number of MED effects and maximum temperature of demineralized water. Results for $\Delta T_{effects} = 4°C$.

Table 8
Techno-Economic results of the CSP + D plants proposed in this work.

	$CO_2 + C_6F_6$ Simple	$CO_2 + C_6F_6$ Precompressed	$CO_2 + C_6F_6$ Cascade	sCO_2 Recompressed
	CSP plant results			
Yearly Electric Energy [GWh$_{el}$/year]	407.9	414.9	395.5	404.0
Yearly Energy to MED [GWh$_{th}$/year]	581.1	562.9	620.2	576.5
TES Size [h]	8	8	8	8
Equivalent Hours of Defocusing [h/year]	74	122	14	83
Solar Multiple	2.51	2.59	2.36	2.53
Specific CSP CAPEX [\$/kW$_{el}$]	5158	5265	5035	5530
LCOE [\$/MWh$_{el}$]	131	131	132	139
	MED plant results (8 effects, $\Delta T_{effects} = 3°C$)			
EOH [h/year]	4069	4149	3955	4040
LCOW [\$/m³]	1.56	1.56	1.58	1.44
Annual fresh water [Mm³/year]	3.58	3.54	3.74	4.22

plant is installed. To increase the generalisation of the study, the LCOW has been calculated at three annual EOH which can be representative of both peaker plants and baseload plants, or to make possible the evaluation at different geographical locations and solar field design. The results of LCOW at different annual EOH are presented in Fig. 9 for the case with 3 °C of temperature difference between effects, and in Fig. 10 for the case of 4 °C effects temperature difference. From the results it is possible to notice a strong dependence of the LCOW on the EOH.

For the specific analysis of this work, the MED plants are proposed with 8 effects and an average apparent difference between the latent effects of 3 °C, representing the most favourable configuration for the LCOW. According to the LCOE analysis, the optimal TES size is obtained at 8 equivalent hours, for all the power cycle configurations. The yearly results are proposed in Table 8 in terms of electric energy produced (accounting for the generators and motors electromechanical efficiency of 99%, as showed in Table 4), thermal rejected energy to the desalination plant and some other key performance parameters of the CSP plant. Considering the nature of the cogenerative plant, the resulting energy produced does not include any electric consumption related to the power cycle heat rejection system (it is allocated to the operating costs of the MED), but includes the yearly energy absorbed by the HTF pump, computed according to the results of Fig. 3, and specific to each HTF temperature range of Table 5. As the resulting performances of the MED plant are strictly related to the operating conditions of the CSP plant (in terms of yearly rejected energy, annual EOH, temperature of the demineralized water/heat source), they are also presented in the bottom of Table 8.

From an energetic perspective, the transcritical cycle with the $CO_2 + C_6F_6$ mixture (particularly in the precompression layout) shows higher electric performances than the sCO_2 counterpart, with + 3% in energy production and a lower specific CAPEX, with LCOE reductions up to 6%.

Regarding the freshwater production, the sCO_2 cycle can definitely benefit from a lower thermal specific consumption: a value around 135 kWh/m³, 10% lower than the one of the $CO_2 + C_6F_6$ mixture (near 150 kWh/m³). Accordingly, the freshwater production for the sCO_2 plant is higher on a yearly basis, and lower LCOW are computed (1.44 \$/m³ against the 1.56 \$/m³ of the mixture power plant). In fact, the different heat rejection temperature from the HRU of the two power cycles is the consequence of these results, benefiting the sCO_2 power cycle. Additional comments to the results and few comparisons with literature results are available in Appendix E.

Conclusions

By adopting a cogenerative CSP + D system based on the MED technology and innovative CO_2-based power cycles it is possible to fully exploit the rejected heat from a high-minimum temperature closed power cycle without affecting its thermal efficiency, avoiding the parasitic electric consumptions of air-cooled HRU: this approach marks a significant difference with respect to the state of the art of CSP + D plants based on steam cycles, that feed the MED through bleeding from the steam turbine. Differently from the literature exploring sCO_2 power blocks, in this work the totality of the heat rejected from the power cycle of a CSP plant is introduced in the desalination plant, due to the high value of minimum temperature of the power cycle at design, a condition in which CO_2-mixtures have electrical performances higher than sCO_2 cycles.

With respect to other solar desalination systems (like RO coupled with photovoltaic plants), with a CSP + MED system the waste product of the power production section can be adopted as input to the desalination plant, evidencing the inherent excellent integration capability of these two systems. As results, specific thermal energy consumptions

around 130–150 kWh/m³ are computed with CO_2-based cycles, per unit of desalinated water: these levels are twice the range achieved with steam cycles, but are obtained without electric power loss from the electric side, as no bleedings are foreseeable in CO_2 plants.

An annual analysis of a CSP plant with a state-of-the-art solar tower and solar salts as HTF is carried out, adopting specific tools, selecting Sevilla (Spain) as a reference European location with high solar irradiation. According to this analysis, designing the solar plant and fixing the power cycle to a reference size of 100 MW$_{el}$, annual equivalent hours in the order of 4000 h/year are achievable: these values are tied to promising ranges of LCOE (around 130 $/MWh$_{el}$) and specific CAPEX of the overall CSP plants (in the order of 5000 $/kW$_{el}$).

Regarding the power cycle analysis, the innovative CO_2 mixture in transcritical cycles proved to be effective in the reduction of the LCOE of a CSP tower plant by about 6%, with a much simpler cycle layout if compared to the recompressed sCO$_2$, suggesting an easier control and operation of the plant. On the other hand, looking at the MED process, the pure CO_2 plant outperformed the CO_2 mixture in terms of both LCOW and annual distillate production due to the lower thermal energy consumption.

In the scenario analyzed, LCOW in the order of 1.4–1.6 $/m³ are obtained, but LCOW around 1.1–1.2 $/m³ are foreseeable with plants designed in locations characterized by a higher annual radiation and TES capacity, by exploiting capacity factors of the solar plant in the order of 70%.

Future works will develop and asses coupling between another CSP + D technology, not based on the MED but on the forward osmosis, as part of the research on this topic.

Data availability

Data will be made available on request.

Appendix A:. Details on the MED modelling

In this appendix are described some of the hypothesis done in the modelling of the MED plant, along with a focus on a specific condition of MED plant, selected as representative of the technology.

The T-Q diagram proposed in Fig. 11 helps in visualizing the heat transfer process from the demineralized water loop side, assuming an arbitrary configuration of the MED plant, with 4 latent effects and the maximum temperature of the hot source at 85 °C: in the first latent effect, the demineralized water releases most of its energy content to a feed seawater stream allowing it to partially evaporate, with an approach temperature of 3 °C. Then, the temperature of the sensible heat source defines the top brine temperature and the numbers of effects of the MED plant. The rest of thermal energy available from the heat source is then transferred through the feed preheaters and the sensible intermediate effects. The vapour formed in the latent first effect passes through a mesh-wire demister entering the second latent effect and act as a heat source for the subsequent stage, by releasing its latent heat of condensation. Starting from the second latent effect, the main driving force is the temperature difference between the latent effects. The condensed freshwater streams produced in each effect by the sub-atmospheric condensation of the vapour formed in the previous stage are then pumped and collected.
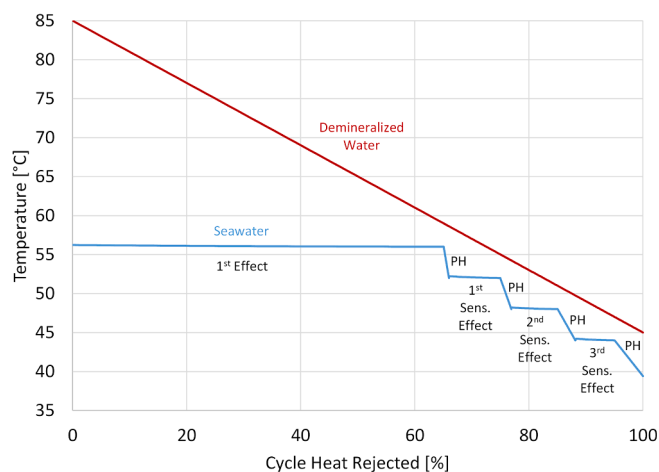

Fig. 11. T-Q diagram of the MED layout proposed in Fig. 1, assuming 4 effects and a maximum temperature of the demineralized water of 85 °C.

The core of the main effects consists of a horizontal falling-film evaporator/condenser tube bank where the condensing steam from the previous effect is condensed inside the tubes and the preheated seawater feed is sprayed on the outer surface of the tubes to evaporate from a liquid film. Other characteristics of the single stage are a bottom un-evaporated brine pool, and a mesh-wire demister for the vapour entering the next effect. Once it is formed, the vapour is subject to a series of pressure drop trough the bundle, the mesh-wire demister, and during in-tube condensation in the next effect. These pressure drops represent thermodynamic losses, since pressure and temperature are strictly related during phase change, which causes a temperature drop during condensation. The total pressure drop in each stage have been computed considering the geometric parameters of a typical low temperature-MED plant [48] to assess the realistic mean temperature difference between the two sides of the evaporator/condenser. The total vapour pressure drop (and then the corresponding temperature drop) is calculated as the sum of the three terms: the pressure drop through the tube bundle, the one in the mesh-wire demister (considering a velocity of the vapour that avoids entrainment [49]), and an average pressure drop during in-tube condensation in the next effect. The correlations adopted are described in the work of Zhou et al. [48]. While the vapour encounters a temperature depression, the temperature of the evaporating sea water sprayed on the bundle undergoes an increase due to boiling point elevation (BPE) that reduces the available mean temperature difference, increasing the area necessary for the evaporator/condenser.

In this work, it is decided not to recirculate the brine since the steam obtainable from its flashing at the entrance to the next stage is computed to be in the order of 1% of the total distillate. Non-equilibrium allowance effects are therefore not treated, even for the absence of flashing boxes. Thus, a brine pool is maintained just to reduce the thermal losses to the environment improving the thermal efficiency of the effect, but the exceeding brine is mixed to the discharged fraction of seawater after the down condenser. Since the amount of discarded seawater is much larger than the amount of brine collected in each effect, this allows to reject into the sea a medium–low temperature water (at about 38 °C) with a low salts content (near the seawater salinity), reducing the environmental impact of the rejected stream.

Appendix B:. Additional information on the design of the CSP plant

The design of the solar field is carried out with the tool SolarPilot. The main solar field characteristics are provided in Table 9. The heliostats aiming strategy "Image Size Priority" with a maximum offset factor of 4 is adopted for the solar field simulation, as it ensures a good compromise between homogeneity of the flux distribution and optical efficiency [50], considering the fixed dimensions of the receiver; the maximum offset is chosen in order to meet a peak heat flux on the receiver of 1 MW/m^2. The simulation in SolarPilot are carried out assuming the sun position at the solar noon of the summer solstice.

As mentioned in the manuscript and reported in Table 2, a receiver circuitation different from the one in Crescent Dunes is studied, for an HTF temperature range of 565–420 °C. Since no existing CSP plant has these characteristics, the receiver circuitation is obtained through a simplified optimization procedure based on the receiver thermal and hydrodynamic performances at design conditions, already adopted in literature by the authors [51]. In detail, the number of tubes per panel, the number of panels per flow path, and the tubes outer diameter are varied aiming at maximizing the so called fictitious thermal power ($\dot{Q}_{fictitious}$). The latter is the thermal power absorbed by the HTF at design conditions depurated from the thermal power required by the power block to produce the electricity needed to run the HTF pumps. For each combination of tubes outer diameter and number of panels per flow path, the number of parallel tubes is determined assuming a distance between the adjacent tubes of 2 mm; then, $\dot{Q}_{fictitious}$ is computed through Equation (3) where $\dot{Q}_{in\,rec,design}$ is the receiver thermal input, η_{th} is the receiver design thermal efficiency, $P_{HTF,pump}$ is the electric power consumed by the HTF circulation pump at design conditions (assuming a pump efficiency of 80%), and η_{cycle} is the power cycle nominal efficiency.

$$\dot{Q}_{fictitious} = \dot{Q}_{inrec,design} \cdot \eta_{th} - \frac{P_{HTF,pump}}{\eta_{cycle}} \tag{3}$$

For each combination of tubes diameters and number on panels, η_{th} and $P_{HTF,pump}$ are obtained, assuming an HTF temperature at the receiver inlet of 420 °C, through the Modelica package SolarReceiver2D [32], that computes also the HTF pressure drop across the receiver. The latter is a two-dimensional dynamic thermal model that allows simulation of any type of external cylindrical receiver. η_{cycle} is assumed equal to 42% that represents the average value of the power cycle efficiencies computed in this work for the configurations adopting the HTF temperature range of 420–565 °C. The thermal model is run assuming a wind speed of 5.8 m/s, which is an average value on the top of the tower in the plant location [52]. The resulting receiver characteristics are reported in Table 2, highlighting that a low temperature variation of the HTF within the receiver makes convenient the adoption of a lower number of tubes per panel, with a larger tube diameter. Despite the receiver design optimization is carried considering a HTF temperature at the receiver inlet of 420 °C, the obtained receiver characteristics are adopted also for the cases with inlet temperature 415 °C and 432 °C (see Table 2).

Table 9
Main solar field characteristics modelled in SolarPilot.

Parameter	Value
Heliostats dimensions [m]	11.3 × 10.4
Heliostats number	10,924
Tower height (including the receiver) [m]	195
Heliostats reflectivity / fouling factor [%]	95 / 95
Heliostats surface slope error [mrad]	1.53

Appendix C:. Description of the power block layouts

The computational tool adopted in this work for the simulations of the power cycle performances is Aspen Plus, a commercial software applied for modelling chemical processes and power cycles for several applications, which integrates mass and energy balances with dedicated equations of state as well as several specific component parameters starting from a component library or user-defined components model.

As mentioned, the CSP plant adopts a direct storage system, meaning that the HTF and the storage fluid coincide with the same heat transfer medium (solar salts). Four power block layouts are considered for the simulation of the innovative CO2-based cycles: the simple recuperative cycle, the recompressed cycle, the precompressed cycle and the cascade cycle, depicted in Fig. 4. As a matter of fact, a previous literature work developed within the SCARABEUS project evidenced that all these power block layouts present similar techno-economic effectiveness, when implemented in a CSP plant with a CO2-based working fluid [35].

The simple recuperative cycle consists of a compression step to increase the pressure of the mixture from saturated liquid conditions to the maximum cycle pressure (from 1 to 2), followed by the working fluid preheating in the recuperator (PCHE) (from 2 to 3), reaching the maximum cycle temperature after the primary heat exchanger (PHE) (point 4). The mixture is then expanded in the turbine (from 4 to 5) and partially cooled down in the recuperator, where it can also partially condense (from 5 to 6), before entering the condenser (COND). An example of the T-s (Temperature-Entropy) diagram for a selected mixture is reported in Fig. 5.

In the benchmark layout, the recompression cycle (REC), with pure sCO$_2$ the pump is replaced by a compressor and the pre-heating section is split in two recuperators that works at different temperature (LT and HT PCHE) and with a different mass flow rate to compensate the effects of the unbalanced heat capacities of CO2-based fluid across the low-pressure side of the recuperator, at low temperature. The sCO$_2$ is compressed (from 1 to 2) to reach the maximum cycle pressure and enters the LT recuperator to preheat (from 2 to 3) and mixed (from 3 to 4) with the fraction of CO$_2$ that is re-compressed (from 10 to 11). After mixing, sCO$_2$ is preheated in the HT PCHE recuperator, reaching the maximum temperature in the PHE, before the expansion that occurs in the turbine (from 6 to 7). The turbine outlet flow is used to preheat the high-pressure side in the HT and LT PCHE recuperator, then it is split: a fraction is compressed (from 10 to 11), while the other fraction is cooled in the HRU (from 12 to 1) up to the minimum cycle temperature.

The other two layouts (precompression and cascade) have been already presented for CO$_2$ mixtures in previous works as an alternative to the simple transcritical cycle [36,34]. The cascade is characterized by a partial preheating phase of the working fluid (from 2 to 3), which allows a low temperature at the PHE inlet (point 4) and, consequently, a higher temperature difference across the PHE (from 4 to 5) to reach the designed turbine inlet temperature. This is reflected in a higher temperature difference of the HTF, as reported in Table 5: the cascade layout aims at the maximization of the heat recovery from the heat source. In the precompression cycle, the turbine outlet pressure (point 6) is the one that optimize the cycle efficiency. The turbine outlet flow preheats the high-pressure side in the HT recuperator (from 6 to 7), then the flow is compressed (from 7 to 8) to a pressure that is compatible with the bubble pressure at 51 °C (point 1) and the pressure losses within the LT recuperator and condenser.

One of the best features of the adoption of a CO2-based mixture is the capability to operate with good cycle efficiency even in a simple recuperative layout, where only one Printed Circuit Heat Exchanger (PCHE) recuperator and one compression step are necessary, thanks to the well-balanced heat capacities in the recuperator.

Appendix D:. Results on solar plant annual analysis

The results in this appendix refer to the off-design and yearly analysis of the CSP plant located in Sevilla. In particular, in Fig. 12 it is reported the trend of the solar field optical efficiency for any sun position: according to the design criteria, the solar field is sized at the solar noon of the summer solstice. From the optical efficiency map it is possible to notice that an optical efficiency of around 62% at design is computed for this CSP plant. The results of Fig. 13, instead, show the solar resources of the location, as a daily average for each month, for a representative year. In addition, the daily average across each month of the thermal power delivered to the HTF is also shown, computed according to the methodology of Fig. 7.
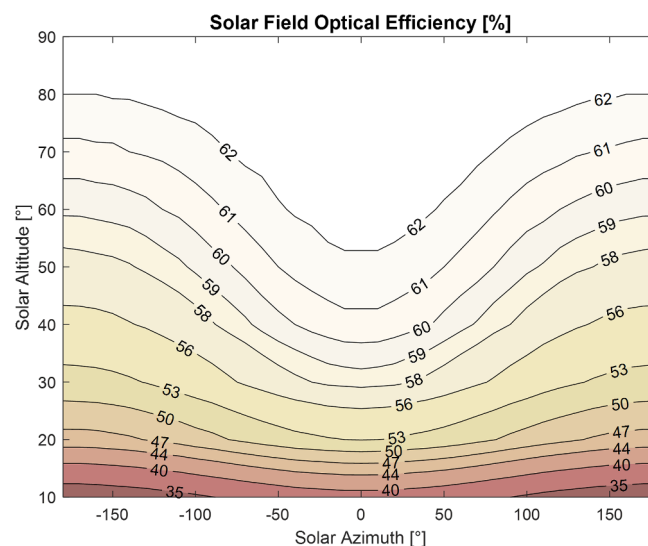

Fig. 12. Off-design map of the optical efficiency of the solar field proposed in this work in Fig. 2.
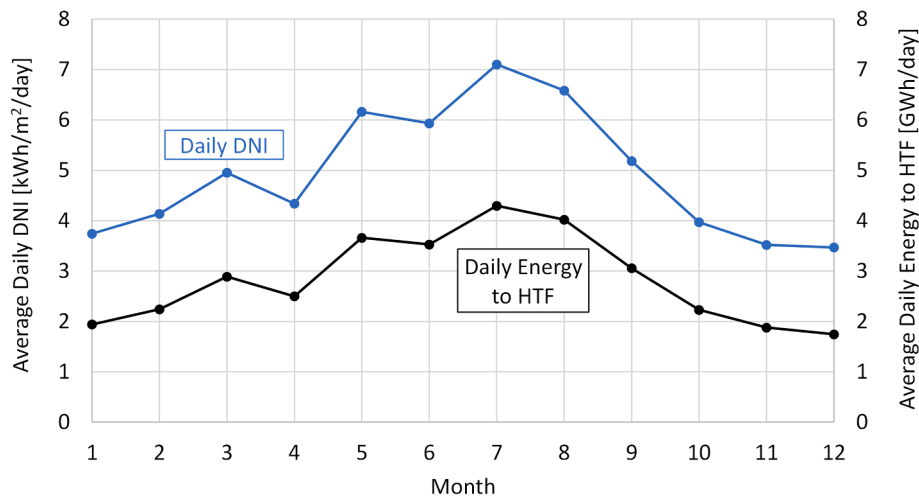
Fig. 13. Average monthly DNI data of Sevilla (Spain) taken from the SolarPilot database, with an yearly average value of 4.92 kWh/m²/day. Average monthly thermal energy transferred to the HTF from the solar plant considered.

Appendix E:. Additional results discussion

This appendix is dedicated to an additional analysis of the results of this work, proposed in Table 8. For comparison purposes, Hoffmann [47] analysed a state-of-the-art 100 MW$_{el}$ CSP + MED tower plant with the MED unit driven by the condenser of the steam Rankine cycle at different condensation temperatures (60–75 °C) with LCOW in the range 3.6–2.6 $/m³ and the LCOE within the range 152–160 $/MWh$_{el}$, which are numbers not as profitable as the one of this work, even if the location (Arandis, Namibia) is characterized by higher annual DNI (2528 kWh/m²/year). Moreover, Hoffmann concluded that the proposed CSP + MED solution could not be competitive against grid-powered RO option (1.78 $/m³) in his case-study. In the state-of-the-art CSP + MED solution, the heat is provided to the MED system by bleeding a fraction of the steam from the turbine or by the condenser (raising the cycle minimum temperature to 60–75 °C) with associated electrical production loss. Instead, in the proposed technology there is no need to compromise the electrical production (and the LCOE) to achieve good results for the desalinated water production, since the heat introduced in the MED is the total amount of the heat naturally rejected from the cycle in the HRU. The results of this work can be also compared to conditions of sCO$_2$ cycles applied in CSP + MED cogenerative plants with a lower value of minimum temperature of the cycle temperature: in fact, the choice of this work to adopt a higher value of compression inlet temperature (more representative of hot environments) allows the 100% conversion of the thermal duty entering the power block for electrical and desalinated water productions. Under this perspective, Sharan et al. [26] reported that a 6-effects CSP + MED plant with pure sCO$_2$ can reach a distillate production of 4′472 m³/day at similar thermal duty available, which is remarkably lower than the annual freshwater production of 4.22 million m³/year obtained in this work for pure sCO$_2$ (Table 8), where the equivalent daily production would be 11′562 m³/day. Without discussing the cost assumptions that could differ from previous research works, and considering that the CAPEX of the MED system in inversely proportional to the distillate production [39], the solution proposed in this work seems more cost-effective.

References

[1] Burek et al., P. The Water Futures and Solutions Initiative of IIASA. 2016, p. 23–26.

[2] UNESCO. The United Nations World Water Development Report 2018: Nature-Based Solutions for Water. 2018.

[3] Eke J, Yusuf A, Giwa A, Sodiq A. The global status of desalination: An assessment of current desalination technologies, plants and capacity. Desalination 2020;495 (March):114633. https://doi.org/10.1016/j.desal.2020.114633.

[4] Mabrouk AN, Fath HES. Technoeconomic study of a novel integrated thermal MSF-MED desalination technology. Desalination 2015;371:115–25. https://doi.org/10.1016/j.desal.2015.05.025.

[5] Almulla Y. Gulf Cooperation Council (GCC) countries 2040 energy scenario for electricity generation and water desalination Yousef Almulla-Almulla@kth.se Student MSc Sustainable Energy Engineering. 2014.

[6] Villacorte LO, Tabatabai SAA, Anderson DM, Amy GL, Schippers JC, Kennedy MD. Seawater reverse osmosis desalination and (harmful) algal blooms. Desalination 2015;360:61–80. https://doi.org/10.1016/j.desal.2015.01.007.

[7] Delgado-Torres AM, García-Rodríguez L. Solar Desalination Driven by Organic Rankine Cycles (Orc) and Supercritical CO 2 Power Cycles: An Update. Processes 2022;10(1):153.

[8] Gentile G, Manzolini G. The Value of CSP with Thermal Energy Storage in Providing Flexible Electric Power. In: Sustainable Energy Development and Innovation: Selected Papers from the World Renewable Energy Congress (WREC). Springer Nat 2020;2022:103–9. https://doi.org/10.1007/978-3-030-76221-6_15.

[9] Binotti M, Astolfi M, Campanari S, Manzolini G, Silva P. Preliminary assessment of sCO2 cycles for power generation in CSP solar tower plants. Appl Energy Oct. 2017;204:1007–17. https://doi.org/10.1016/J.APENERGY.2017.05.121.

[10] SCARABEUS. No Title. Supercritical Carbon dioxide/Alternative fluids Blends for Efficiency Upgrade of Solar power plants; 2019. https://www.scarabeusproject.eu/.

[11] Binotti M, Di Marcoberardino G, Iora P, Invernizzi C, Manzolini G. Scarabeus: Supercritical carbon dioxide/alternative fluid blends for efficiency upgrade of solar power plants. AIP Conf Proc 2020;2303(December). https://doi.org/10.1063/5.0028799.

[12] G. Manzolini et al., "Adoption of CO2 blended with C6F6 as working fluid in CSP plants," in AIP Conference Proceedings, AIP Publishing LLCAIP Publishing, May 2022, p. 090005. doi: 10.1063/5.0086520.

[13] Di Marcoberardino G, et al. Experimental characterisation of CO2 + C6F6 mixture: Thermal stability and vapour liquid equilibrium test for its application in transcritical power cycle. Appl Therm Eng Jul. 2022;212. https://doi.org/10.1016/J.APPLTHERMALENG.2022.118520.

[14] Masoud Parsa S, Majidniya M, Alawee WH, Dhahad HA, Muhammad Ali H, Afrand M, et al. Thermodynamic, economic, and sensitivity analysis of salt gradient solar pond (SGSP) integrated with a low-temperature multi effect desalination (MED): Case study, Iran. Sustainable Energy Technol Assess 2021;47. https://doi.org/10.1016/j.seta.2021.101478.

[15] Cunha DPS, Pontes KV. Desalination plant integrated with solar thermal energy: A case study for the Brazilian semi-arid. J Clean Prod 2022;331(November). https://doi.org/10.1016/j.jclepro.2021.129943.

[16] Ahmed F, Sharizal Abdul Aziz M, Palaniandy P, Shaik F. A review on application of renewable energy for desalination technologies with emphasis on concentrated solar power. Sustainable Energy Technol Assess 2022;53. https://doi.org/10.1016/j.seta.2022.102772.

[17] Moser M, Trieb F, Fichter T. Potential of concentrating solar power plants for the combined production of water and electricity in MENA countries. J Sustain Dev Energy Water Environ Syst 2013;1(2):122–40. https://doi.org/10.13044/j.sdewes.2013.01.0009.

[18] Palenzuela P, Alarcón-Padilla DC, Zaragoza G, Blanco J. Comparison between CSP +MED and CSP+RO in Mediterranean Area and MENA Region: Techno-economic Analysis. Energy Procedia 2015;69:1938–47. https://doi.org/10.1016/j.egypro.2015.03.192.

[19] Sankar D, Deepa N, Rajagopal S, Karthik KM. Solar power and desalination plant for carbon black industry: Improvised techniques. Sol Energy 2015;119:243–50. https://doi.org/10.1016/j.solener.2015.07.001.

[20] Olwig R, Hirsch T, Sattler C, Glade H, Schmeken L, Will S, et al. Techno-economic analysis of combined concentrating solar power and desalination plant configurations in Israel and Jordan. Desalination Water Treat 2012;41(1-3):9–25.

[21] Askari IB, Ameri M, Calise F. Energy, exergy and exergo-economic analysis of different water desalination technologies powered by Linear Fresnel solar field. Desalination 2018;425(July). https://doi.org/10.1016/j.desal.2017.10.008.

[22] Moradi M, Ghorbani B, Shirmohammadi R, Mehrpooya M, Hamedi MH. Developing of an integrated hybrid power generation system combined with a multi-effect desalination unit. Sustainable Energy Technol Assess 2019;32 (November). https://doi.org/10.1016/j.seta.2019.02.002.

[23] C. Sommariva, "Desalination and advanced water treatment : economics and financing," 2010.

[24] Sharaf MA, Nafey AS, García-Rodríguez L. Thermo-economic analysis of solar thermal power cycles assisted MED-VC (multi effect distillation-vapor compression) desalination processes. Energy 2011;36(5):2753–64. https://doi.org/10.1016/j.energy.2011.02.015.

[25] Yuan L, Zhu Q, Zhang T, Duan R, Zhu H. Performance evaluation of a co-production system of solar thermal power generation and seawater desalination. Renew Energy 2021;169:1121–33. https://doi.org/10.1016/j.renene.2021.01.096.

[26] Sharan P, Neises T, Turchi C. Thermal desalination via supercritical CO 2 Brayton cycle : Optimal system design and techno-economic analysis without reduction in cycle efficiency. Appl Therm Eng 2019;152(December). https://doi.org/10.1016/j.applthermaleng.2019.02.039.

[27] Saravi SS, Tassou SA. An investigation into sCO2 compressor performance prediction in the supercritical region for power systems. Energy Procedia 2019; 161:403–11.

[28] Aspen Technology Inc., "Aspen Plus®, Version V12.1." 2022.

[29] Baccioli A, Antonelli M, Desideri U, Grossi A. Thermodynamic and economic analysis of the integration of Organic Rankine Cycle and Multi-Effect Distillation in waste-heat recovery applications. Energy 2018;161:456–69. https://doi.org/10.1016/j.energy.2018.07.150.

[30] Wagner MJ, Wendelin T. SolarPILOT: A power tower solar field layout and characterization tool. Sol Energy 2018;171:185–96.

[31] SolarReserve, "Crescent Dunes Solar Energy Plant," 2014.

[32] Gentile G, Picotti G, Casella F, Binotti M, Cholette ME, Manzolini G. SolarReceiver2D: a Modelica Package for Dynamic Thermal Modelling of Central Receiver Systems. IFAC-PapersOnLine 2022;55(20):259–64. https://doi.org/10.1016/j.ifacol.2022.09.105.

[33] Alfani D, Astolfi M, Binotti M, Silva P, Macchi E. Off-design Performance of CSP Plant Based on Supercritical CO2 Cycles. AIP Conf Proc 2020;2303(December). https://doi.org/10.1063/5.0029801.

[34] Morosini E, Ayub A, di Marcoberardino G, Invernizzi CM, Iora P, Manzolini G. Adoption of the CO2 + SO2 mixture as working fluid for transcritical cycles: A thermodynamic assessment with optimized equation of state. Energy Convers Manag 2022;255:115263. https://doi.org/10.1016/j.enconman.2022.115263.

[35] Morosini E, Villa E, Quadrio G, Binotti M, Manzolini G. Solar tower CSP plants with transcritical cycles based on CO2 mixtures: A sensitivity on storage and power block layouts. Sol Energy 2023;262:111777.

[36] Crespi F, Rodríguez de Arriba P, Sánchez D, Ayub A, Di Marcoberardino G, Invernizzi CM, et al. Thermal Efficiency Gains Enabled by Using CO2 Mixtures in Supercritical Power Cycles. Energy 2022;238. https://doi.org/10.1016/j.energy.2021.121899.

[37] Span R, Wagner W. A New Equation of State for Carbon Dioxide Covering the Fluid Region from the Triple-Point Temperature to 1100 K at Pressures up to 800 MPa. J Phys Chem Ref Data 1996;25(6):1509–96.

[38] Di Marcoberardino G, Morosini E, Manzolini G. Preliminary investigation of the in fluence of equations of state on the performance of CO2 + C6F6 as innovative working fluid in transcritical cycles. Energy 2022;238:121815. https://doi.org/10.1016/j.energy.2021.121815.

[39] Papapetrou M, Kosmadakis G, Cipollina A, La Commare U, Micale G. Industrial waste heat: Estimation of the technically available resource in the EU per industrial sector, temperature level and country. Appl Therm Eng 2018;138(July 2017): 207–16. https://doi.org/10.1016/j.applthermaleng.2018.04.043.

[40] M. Hasan, K. Manesh, R. S. Ghadikolaei, and H. V. Modabber, "Integration of a Combined Cycle Power Plant with MED-RO Desalination Based on Conventional and Advanced Exergy ," 2021.

[41] Druetta P, Mussati S. Minimizing the total cost of multi effect evaporation systems for seawater desalination. Desalination 2014;344:431–45. https://doi.org/10.1016/j.desal.2014.04.007.

[42] N. T. Weiland, B. W. Lance, and S. R. Pidaparti, "sCO2 Power Cycle Component Cost Correlations From DOE Data Spanning Multiple Scales and Applications," in Turbo Expo: Power for Land, Sea, and Air, vol. Volume 9: 2019. doi: 10.1115/GT2019-90493.

[43] "Thermoflow Inc., Thermoflex, (2021).".

[44] Kelly B, Izygon M, Vant-Hull L. Advanced Thermal Energy Storage for Central Receivers with supercritical coolants. SolarPaces Conf 2010. https://doi.org/10.2172/981926.

[45] "System Advisor Model (SAM)." https://sam.nrel.gov/.

[46] Manzolini G, Lucca G, Binotti M, Lozza G. A two-step procedure for the selection of innovative high temperature heat transfer fluids in solar tower power plants. Renew Energy 2021;177:807–22. https://doi.org/10.1016/j.renene.2021.05.153.

[47] Hoffmann JE, Dall EP. Integrating desalination with concentrating solar thermal power: A Namibian case study. Renew Energy 2018;115:423–32. https://doi.org/10.1016/j.renene.2017.08.060.

[48] Zhou S, Guo Y, Mu X, Shen S. Effect of design parameters on thermodynamic losses of the heat transfer process in LT-MEE desalination plant. Desalination 2015;375: 40–7. https://doi.org/10.1016/j.desal.2015.07.015.

[49] El-Dessouky HT, Alatiqi IM, Ettouney HM, Al-Deffeeri NS. Performance of wire mesh mist eliminator. Chem Eng Process 2000;39(2):129–39. https://doi.org/10.1016/S0255-2701(99)00033-1.

[50] Gentile G, Picotti G, Binotti M, Cholette ME, Manzolini G. Dynamic thermal analysis and creep-fatigue lifetime assessment of solar tower external receivers. Sol Energy 2022;247:408–31. https://doi.org/10.1016/j.solener.2022.10.010.

[51] Morosini E, Gentile G, Binotti M, Manzolini G. Techno-economic assessment of small-scale solar tower plants with modular billboard receivers and innovative power cycles. J Phys Conf Ser, IOP Publishing, Dec 2022;2385(1). https://doi.org/10.1088/1742-6596/2385/1/012109.

[52] "Global wind atlas," Global Wind Atlas, 2022. https://globalwindatlas.info/en/.